

# Uni3R: Unified 3D Reconstruction and Semantic Understanding via Generalizable Gaussian Splatting from Unposed Multi-View Images

Xiangyu Sun<sup>1\*</sup>, Haoyi Jiang<sup>2\*</sup>, Liu Liu<sup>4</sup>, Seungtae Nam<sup>3</sup>, Gyeongjin Kang<sup>1</sup>, Xinjie Wang<sup>4</sup>, Wei Sui<sup>5</sup>, Zhizhong Su<sup>4</sup>, Wenyu Liu<sup>2</sup>, Xinggong Wang<sup>2</sup>, Eunbyung Park<sup>3†</sup>

<sup>1</sup>Sungkyunkwan University  
<sup>2</sup>Huazhong University of Science & Technology  
<sup>3</sup>Yonsei University  
<sup>4</sup>Horizon Robotics  
<sup>5</sup>D-Robotics

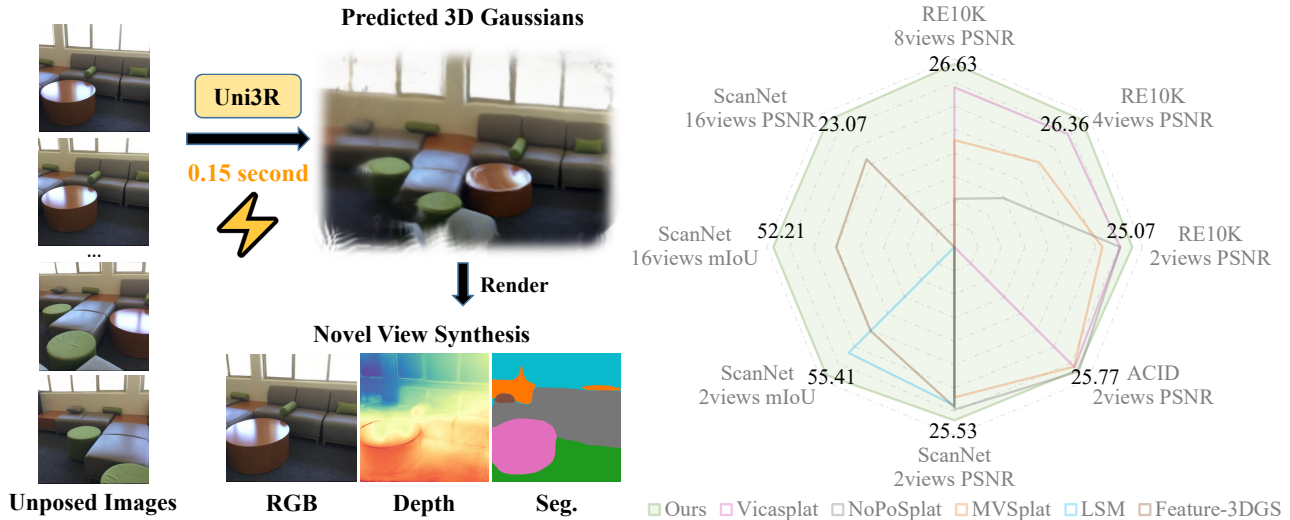


Figure 1: Uni3R takes unposed multi-view images as input and produces a unified 3D Gaussian scene representation, enabling state-of-the-art performance in view synthesis, semantic segmentation, and depth estimation within a single forward pass.

## Abstract

Reconstructing and semantically interpreting 3D scenes from sparse 2D views remains a fundamental challenge in computer vision. Conventional methods often decouple semantic understanding from reconstruction or necessitate costly per-scene optimization, thereby restricting their scalability and generalizability. In this paper, we introduce **Uni3R**, a novel feed-forward framework that jointly reconstructs a unified 3D scene representation enriched with open-vocabulary semantics, directly from unposed multi-view images. Our approach leverages a Cross-View Transformer to robustly integrate information across arbitrary multi-view inputs, which then regresses a set of 3D Gaussian primitives endowed with semantic feature fields. This unified representation facilitates high-fidelity novel view synthesis, open-vocabulary 3D semantic segmentation, and depth prediction—all within a single, feed-forward pass. Extensive experiments demonstrate that Uni3R establishes a new state-of-

the-art across multiple benchmarks, including **25.07** PSNR on RE10K and **55.84** mIoU on ScanNet. Our work signifies a novel paradigm towards generalizable, unified 3D scene reconstruction and understanding. The code is available at <https://github.com/HorizonRobotics/Uni3R>.

## 1 Introduction

The ability to perceive and interpret the 3D world from sparse images is a cornerstone of computer vision, holding profound implications for robotics, autonomous driving, and augmented reality. While significant progress has been made in 3D reconstruction, led by photorealistic methods such as Neural Radiance Fields (NeRF) (Mildenhall et al. 2020), 3D Gaussian Splatting (3DGS) (Kerbl et al. 2023), their reliance on time-consuming, per-scene optimization critically limits their generalizability to novel scenes. In response, a prominent class of generalizable 3D reconstruction methods (Yu et al. 2021; Charatan et al. 2024; Chen et al. 2024; Liu et al. 2024; Xu et al. 2025) has emerged, which learn geometric priors across diverse scenes to perform feed-forward 3D re-

\*Equal contribution, work done during internship at Horizon Robotics.

†Corresponding author.

construction in a feed-forward manner.

While promising, these methods typically focus exclusively on geometry and appearance, overlooking the semantic richness crucial for holistic scene understanding. Recent efforts, including LangSplat (Qin et al. 2024) and Feature-3DGS (Zhou et al. 2024), have incorporated semantic fields into 3D Gaussian Splatting, yet remain constrained by scene-specific optimization and lack scalability in real-world, zero-shot applications. More recently, approaches such as LSM (Fan et al. 2024) and UniForward (Tian et al. 2025) have aimed to unify semantic and radiance fields to jointly infer geometry, appearance, and semantics. However, these methods are built upon DUST3R (Wang et al. 2024a), which is inherently designed for two-view inputs. Consequently, extending them to multi-view scenarios requires expensive pairwise feature matching across views, compromising efficiency and leading to inconsistent reconstructions due to the absence of global 3D context.

To address these limitations, we propose Uni3R, a novel, generalizable framework that synthesizes a unified 3D representation from arbitrary multi-view images for both high-fidelity rendering and dense, open-vocabulary semantic understanding. Leveraging a Cross-View Transformer effectively fuses information across views and produces globally consistent representations, Uni3R predicts unified 3D Gaussian primitives enriched with open-vocabulary semantic features. These Gaussian representations can be seamlessly rendered in real-time to synthesize novel views, supervised solely with source images and bypassing the need for per-scene optimization. Simultaneously, the embedded semantic features enable zero-shot 3D semantic segmentation by querying the scene with arbitrary text prompts.

To further enhance the geometric fidelity of reconstruction, we introduce a point-map-guided geometric loss that improves structural consistency by aligning with pre-trained geometry foundation model. Specifically, we employ a frozen VGGT (Wang et al. 2025) to generate dense point maps along with associated confidence scores, which serve as soft priors to guide the spatial distribution of the 3D Gaussians.

Our contributions are summarized as follows:

- We introduce Uni3R, a novel feed-forward architecture that unifies 3D reconstruction and semantic understanding. It predicts a set of Gaussian primitives with jointly integrated geometry, appearance, and open-vocabulary semantics in a single pass, eliminating the need for per-scene optimization.
- We demonstrate that a powerful geometry foundation model can be effectively extended beyond geometric estimation to support both photometric reconstruction and 3D scene understanding. Its cross-frame attention mechanism enables robust feature fusion to produce globally consistent scene representations from an arbitrary number of input views, while its predicted point maps provide potent geometric guidance.
- Uni3R achieves state-of-the-art performance across multiple tasks, including novel view synthesis, open-vocabulary 3D semantic segmentation, and depth predic-

tion on the challenging RE10K (Zhou et al. 2018) and ScanNet (Dai et al. 2017) datasets, underscoring its superior generalization and versatility.

## 2 Related Work

### 2.1 Differentiable Neural Representations

Traditional 3D reconstruction methods, such as Structure-from-Motion (SfM) (Dellaert et al. 2000) and Multi-View Stereo (MVS) (Bleyer, Rhemann, and Rother 2011) decompose the process into sequential steps, including feature matching, camera pose estimation, and geometric reconstruction. While effective, these multi-stage processes can be fragile and prone to error accumulation. The advent of Neural Radiance Fields (NeRF) (Mildenhall et al. 2020) revolutionized novel view synthesis by introducing an end-to-end, differentiable approach that models a scene as a continuous function mapping 5D coordinates to color and volumetric density. More recently, 3D Gaussian Splatting (3DGS) (Kerbl et al. 2023) has emerged as a compelling alternative, representing scenes explicitly with a set of 3D Gaussian primitives. Leveraging a highly efficient differentiable rasterizer, 3DGS supports real-time rendering speeds while maintaining exceptional rendering quality. However, canonical 3DGS relies on point clouds from SfM for initialization and rectified camera poses. Our work builds upon the 3DGS formulation but removes reliance on external tools like COLMAP. By predicting Gaussians in an end-to-end pose-free manner, we enable scalable 3D reconstruction and scene understanding.

### 2.2 Feed-forward 3D Reconstruction

The substantial computational cost of per-scene optimization has motivated the development of 3D feed-forward models. PixelNeRF (Yu et al. 2021) and MVSNerF (Chen et al. 2021) learn scene priors across a large number of training scenes, enabling them to predict radiance fields for novel scenes from only a few input views. Following the success of 3DGS, pixelSplat (Charatan et al. 2024), MVSplat (Chen et al. 2024), Generative Densification (Nam et al. 2025), iLRM (Kang et al. 2025) and DepthSplat (Xu et al. 2025) adapt this generalizable paradigm to predict 3D Gaussian parameters directly. However, these approaches typically necessitate known camera poses to guide the reconstruction. To eliminate this constraint, MAST3R (Leroy, Cabon, and Revaud 2024) and DUST3R (Wang et al. 2024a) demonstrate the feasibility of predicting pixel-aligned 3D point clouds directly from image pairs without explicit pose information. Building on these advances, Splatt3R (Smart et al. 2024) and NoPoSplat (Ye et al. 2025) further advance this pose-free paradigm by predicting 3D Gaussian primitives directly from image pairs. Despite their progress, models based on the DUST3R architecture still require sufficient overlap between image pairs and struggle to integrate globally consistent information, leading to fragmented reconstructions. Uni3R overcomes these limitations by employing a Cross-View Transformer, inspired by VGGT (Wang et al. 2025), to interpret and fuse information from an arbitrary number of

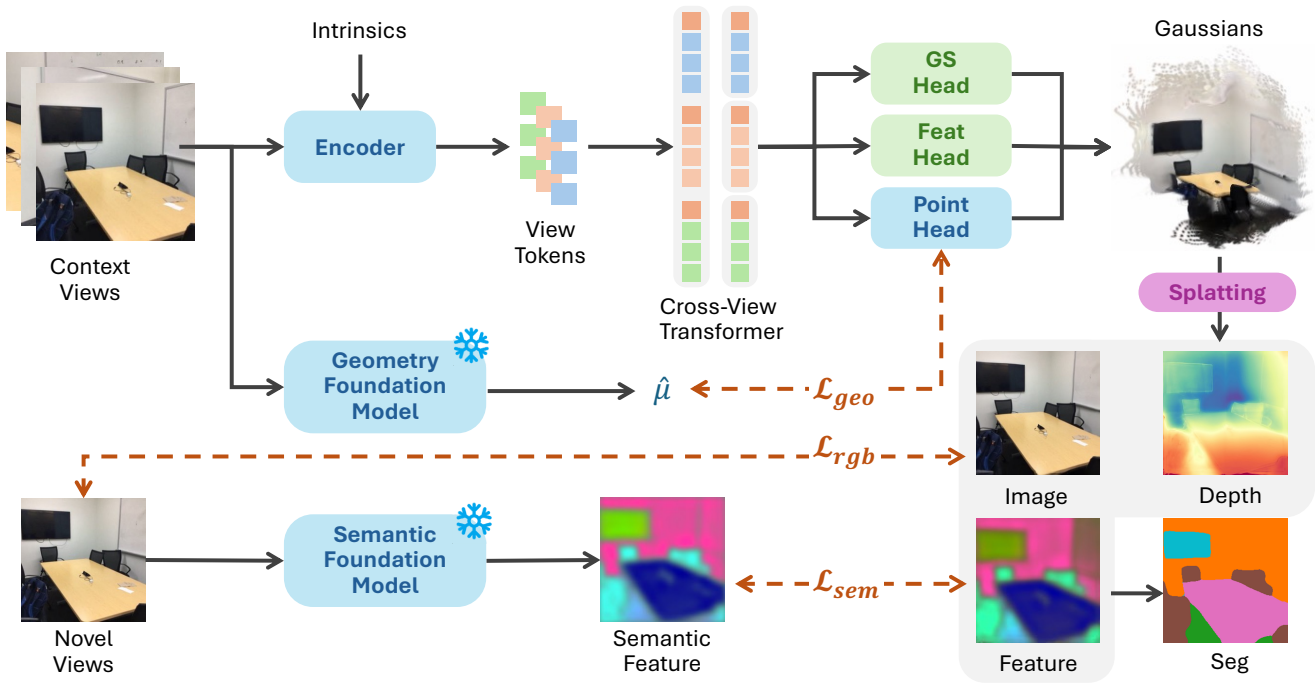


Figure 2: Architectural overview of the Uni3R pipeline for multi-task 3D reconstruction and scene understanding.

views. Based on the globally consistent 3D geometric features, we develop a multi-view, pose-free feed-forward reconstruction model. Our method supports not only image pairs but also extended sequences or video clips, predicting 3D Gaussian primitives in a single forward pass to achieve high-quality, globally coherent 3D reconstruction without requiring camera poses.

### 2.3 Open-Vocabulary Segmentation in 3DGS

Integrating semantics into 3D reconstructions is crucial for higher-level scene understanding tasks. Early methods for 3D semantic segmentation required dense, 3D ground-truth labels, which are scarce and laborious to acquire. The advent of powerful 2D vision-language models like CLIP (Radford et al. 2021; Li et al. 2025a) has spurred the development of open-vocabulary methods that lift 2D understanding into 3D. LERF (Kerr et al. 2023) distills 2D CLIP features into 3D radiance fields. Capitalizing on the rendering efficiency of 3D Gaussian Splatting, several methods (Qin et al. 2024; Zhou et al. 2024; Zhai et al. 2025; Liang et al. 2024) have extended Gaussian representations with semantic features. Nonetheless, these methods still rely on per-scene optimization, making them unsuitable for real-time applications in novel environments. While generalizable approaches like LSM (Fan et al. 2024) and GSemSplat (Wang et al. 2024b) have been proposed, they are typically constrained to two-view inputs, restricting their scalability and robustness in complex scenes. In a related vein, GaussTR (Jiang et al. 2025) explores generalizable Gaussian-based segmentation in the context of occupancy prediction. In contrast, Uni3R integrates open-vocabulary understanding into a general-

izable, multi-view framework, producing globally consistent 3D representation embedded with expressive semantics without requiring any 3D semantic labels.

## 3 Method

This section details our methodology, beginning with the feed-forward Gaussian modeling in Section 3.1. We then describe how to endow Gaussians with semantics in Section 3.2, and conclude with the specifics of the training losses in Section 3.3.

### 3.1 Feed-Forward Gaussian Splatting

**Intrinsic Embedding** To resolve the inherent metric ambiguity in monocular reconstruction caused by unknown focal lengths, we incorporate an intrinsic embedding to provide essential geometric cues. Following NoPoSplat (Ye et al. 2025), we encode each camera’s focal length and principal point with a linear projection. The resulting intrinsic embedding is concatenated channel-wise with the corresponding image before patch tokenization, allowing the network to reason about the geometry-aware information.

**Cross-View Transformer Encoder** Uni3R employs a Cross-View Transformer Encoder, following VGGT, to extract and fuse features from all input images into a consistent, view-agnostic latent representation. Each input view  $I^{(i)}$ , augmented with its intrinsic embedding, is first processed by a pre-trained Vision Transformer, DINOv2 (Oquab et al. 2024), to extract a sequence of patch-level feature tokens. To support arbitrary multi-view inputs while maintaining permutation equivariance, a learnable

camera token is appended to each view’s token sequence. The Cross-View Transformer Encoder consists of a series of Transformer blocks that alternate between intra-frame and cross-frame attention. Intra-frame self-attention operates within each view’s token set, refining the per-view features with local context. Subsequently, cross-frame global attention aggregates tokens from all views to establish correspondences and reason about the global 3D geometry. The output latent tokens from the encoder encapsulate a holistic and globally consistent understanding of the 3D scene.

**Decoding Gaussian Parameters** The fused latent representations are decoded into a dense set of 3D Gaussian primitives with a Dense Prediction Transformer (DPT) (Ranftl, Bochkovskiy, and Koltun 2021) followed by dedicated prediction heads for different Gaussian parameters. DPT progressively refines coarse patch-level features with fine-grained local details from intermediate layers, yielding a dense per-pixel feature map.

Subsequently, we predict the properties of a set of pixel-aligned 3D Gaussians with separate MLP heads. Each primitive is parameterized by:

$$G_j = \{\mu_j, \alpha_j, c_j, s_j, r_j, f_j^{\text{sem}}\}, \quad (1)$$

where  $\mu_j \in \mathbb{R}^3$  denotes the 3D center point,  $s_j \in \mathbb{R}^3$  is the scale,  $r_j \in \mathbb{R}^4$  is the rotation quaternion,  $\alpha_j \in [0, 1]$  is the opacity,  $c_j \in \mathbb{R}^3$  is the color, and  $f_j^{\text{sem}} \in \mathbb{R}^d$  is a high-dimensional semantic feature vector.

The point head is initialized from pre-trained VGGT weights and is further fine-tuned with rendering-based supervision to align with real-world metric scales. Distinct activation functions are applied to the predicted parameters to constrain them to their valid ranges:

$$\alpha_j = \sigma(f_j^\alpha), \quad (2)$$

$$s_j = \exp(f_j^s) \cdot d_{\text{median}}, \quad (3)$$

$$r_j = \text{normalize}(f_j^r), \quad (4)$$

where  $\sigma(\cdot)$  represents the sigmoid activation function, and  $f_j^\alpha$ ,  $f_j^s$ , and  $f_j^r$  are the latents for opacity, scale, and rotation, respectively. The term  $d_{\text{median}}$  is the median depth value computed from the predicted 3D positions, which helps to normalize the scale.

### 3.2 Rendering with Open-Vocabulary Semantics

Once predicted, the set of Gaussians is rendered into novel views using the differentiable 3D Gaussian rasterizer, extended with semantic feature fields. The Gaussian function is described by:

$$G_j(x) = e^{-\frac{1}{2}x^\top \Sigma_j^{-1}x}, \quad (5)$$

where the covariance matrix  $\Sigma_j$  is constructed from the scale  $s_j$  and rotation  $r_j$ . The rendered color  $\hat{I}$  and feature  $\hat{F}$  at each pixel are computed by alpha-blending the properties of all sorted Gaussians that overlap it, taking  $\hat{F}$  as an example:

$$\hat{F} = \sum_i \hat{f}_i^{\text{sem}} \alpha_i \prod_{j=1}^{i-1} (1 - \alpha_j), \quad (6)$$

where  $\hat{f}_j^{\text{sem}}$  is compressed from  $f_j^{\text{sem}}$  by an autoencoder to mitigate the high memory cost of rendering high-dimensional semantic features.

$$\hat{f}_j^{\text{sem}} = \mathcal{F}_{\text{enc}}(f_j^{\text{sem}}), \quad (7)$$

$$\hat{F}' = \mathcal{F}_{\text{dec}}(\hat{F}), \quad (8)$$

where  $\mathcal{F}_{\text{enc}}$  and  $\mathcal{F}_{\text{dec}}$  are the encoder and decoder, respectively. The autoencoder is trained end-to-end to align the rendered features with CLIP-based image features, enabling efficient open-vocabulary semantic reasoning.

During inference, semantic segmentation is performed by computing the cosine similarity between the pixel-wise semantic features and a set of text-derived prototypes. Given a set of text prompts for desired categories (e.g., “wall,” “chair,” “sofa”), CLIP text encoder generates corresponding feature prototypes  $f^{\text{txt}} \in \mathbb{R}^{N_C \times C}$ , where  $N_C$  is the number of categories. The semantic logits  $S$  is then computed by cosine similarity:

$$S_p = \text{softmax}(f^{\text{txt}} \cdot \hat{F}'). \quad (9)$$

### 3.3 Training Objectives

**Photometric Loss ( $\mathcal{L}_{\text{rgb}}$ ).** To ensure that rendered images match the input views, we combine a pixel-wise L1 loss and the LPIPS metric (Zhang et al. 2018):

$$\mathcal{L}_{\text{rgb}} = \sum_{i=1}^N \left( \|\tilde{I}^{(i)} - \hat{I}^{(i)}\|_1 + \lambda_{\text{LPIPS}} \text{LPIPS}(\tilde{I}^{(i)}, \hat{I}^{(i)}) \right), \quad (10)$$

where  $\tilde{I}^{(i)}$  and  $\hat{I}^{(i)}$  denotes the ground-truth image and the rendered image from the  $i$ -th camera viewpoint, respectively, and  $\lambda_{\text{LPIPS}}$  is set to 0.05.

**Semantic Loss ( $\mathcal{L}_{\text{sem}}$ ).** To endow the Gaussians with open-vocabulary capabilities, we distill knowledge from a frozen, pre-trained 2D vision-language model, LSeg (Li et al. 2022). We extract feature maps  $\tilde{F}^{(i)}$  from each input image using the LSeg image encoder. We then enforce alignment between the rendered semantic feature map  $\hat{F}^{(i)'}$  and the 2D CLIP-based features using a cosine similarity loss:

$$\mathcal{L}_{\text{sem}} = \sum_{i=1}^N \left( 1 - \frac{\tilde{F}^{(i)} \cdot \hat{F}^{(i)'}}{\|\tilde{F}^{(i)}\| \cdot \|\hat{F}^{(i)'}\|} \right). \quad (11)$$

This loss lifts rich 2D semantics into the 3D domain, enabling zero-shot semantic understanding without requiring explicit 3D annotations.

**Geometry Loss ( $\mathcal{L}_{\text{geo}}$ ).** To enhance the geometric consistency, particularly around object boundaries, we adopt a point-map regularization strategy inspired by PM-Loss (Shi et al. 2025). Specifically, we leverage a frozen VGGT (Wang et al. 2025) to generate a dense point map  $\hat{\mu}^{(i)} \in \mathbb{R}^{3 \times H \times W}$  to guide geometric supervision. Given that the predictions from VGGT are not uniformly reliable, especially in challenging regions such as reflective surfaces or areas with heavy occlusion, we introduce a confidence-based masking strategy. We extract the confidence map  $C^{(i)}$  from VGGT

Method	Recon. Time↓		Source View				Target View				
	SfM	Per-Scene	mIoU↑	Acc.↑	rel↓	$\tau$ ↑	mIoU↑	Acc.↑	PSNR↑	SSIM↑	LPIPS↓
LSeg	N/A	N/A	0.4701	0.7891	-	-	0.4819	0.7927	-	-	-
NeRF-DFF	20.52s	1min	0.4540	0.7173	27.68	9.61	0.4037	0.6755	19.86	0.6650	0.3629
Feature-3DGS	20.52s	18mins	0.4453	0.7276	12.95	21.07	0.4223	0.7174	24.49	0.8132	0.2293
PixelSplat		0.064s	-	-	-	-	-	-	24.89	0.8392	0.1641
LSM*		0.108s	0.5034	0.7740	<b>3.38</b>	<b>67.77</b>	0.5078	0.7686	24.39	0.8072	0.2506
Ours		0.162s	<b>0.5403</b>	<b>0.8255</b>	3.87	61.37	<b>0.5584</b>	<b>0.8268</b>	<b>25.53</b>	<b>0.8727</b>	<b>0.1380</b>

Table 1: **Quantitative Comparison on ScanNet.** We evaluate performance on novel view synthesis, depth estimation, and open-vocabulary semantic segmentation. (\*) **Unlike LSM, Uni3R is trained without any 3D annotations.**

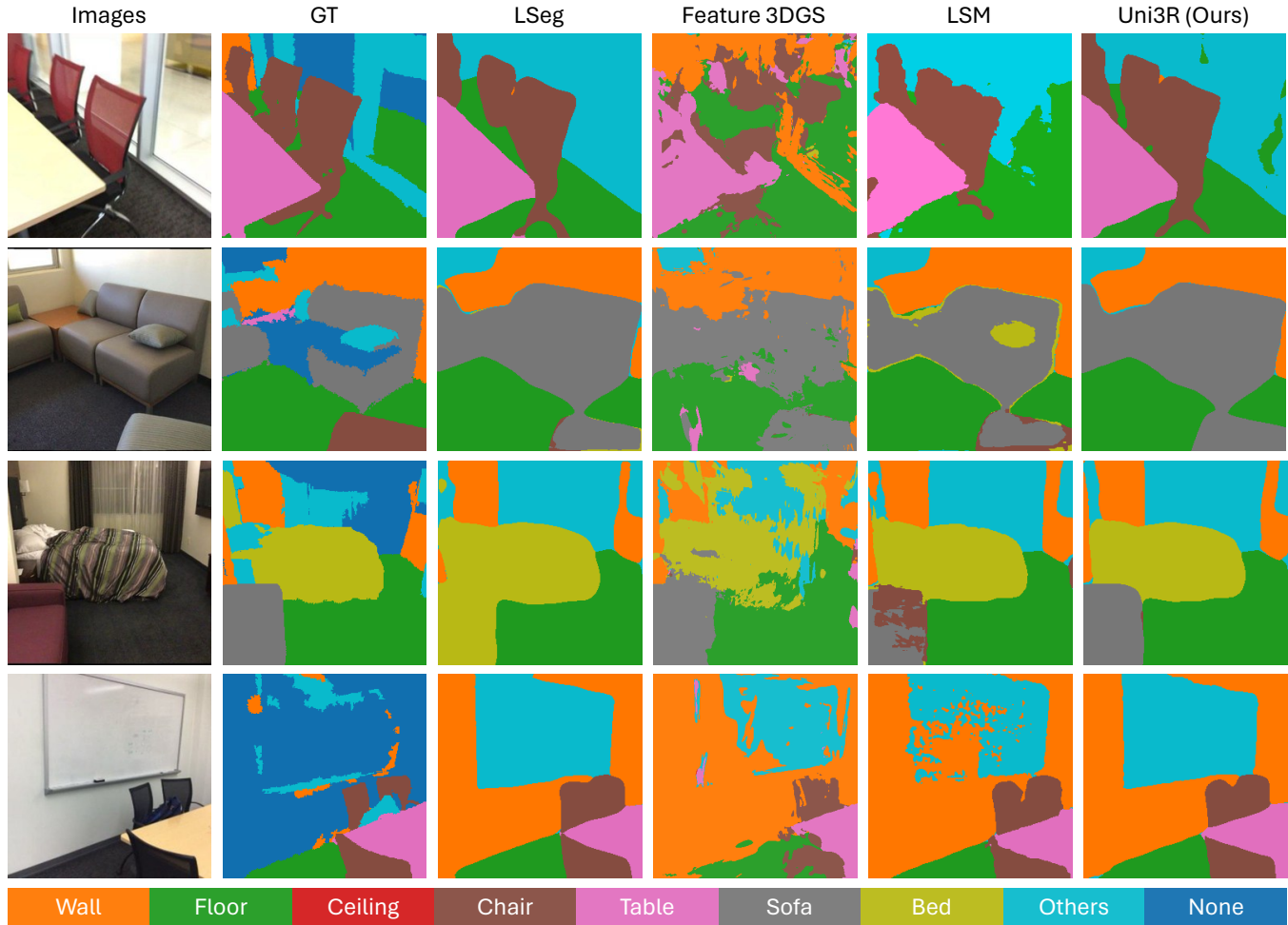


Figure 3: **Qualitative Comparison of Novel-View Segmentation on ScanNet.**

and construct a binary geometry mask,  $M^{(i)} \in \{0, 1\}^{H \times W}$  by selecting the top- $k$  most confident pixels (set as 90% in our experiments). The predicted point maps  $\mu^{(i)}$  from Uni3R are then aligned with  $\hat{\mu}^{(i)}$  via the Umeyama algorithm (Umeyama 1991). Given the masked aligned point clouds  $X_U^{(i)} = \mu^{(i)} \odot M^{(i)}$  and  $X_V^{(i)} = \hat{\mu}^{(i)} \odot M^{(i)}$ , where  $\odot$  denotes the element-wise product, a single-directional

Chamfer distance is computed. The loss is formulated as:

$$\mathcal{L}_{\text{geo}} = \sum_{i=1}^N \frac{1}{N_{\text{pts}}^{(i)}} \sum_{x \in X_U^{(i)}} \min_{x' \in X_V^{(i)}} \|x - x'\|_2^2 \quad (12)$$

$N_{\text{pts}}^{(i)}$  is the total number of points. The final training objective is a weighted sum of the individual losses:

$$\mathcal{L}_{\text{total}} = \mathcal{L}_{\text{rgb}} + \lambda_{\text{sem}} \mathcal{L}_{\text{sem}} + \lambda_{\text{geo}} \mathcal{L}_{\text{geo}}, \quad (13)$$

where the balancing hyperparameters  $\lambda_{\text{sem}}$  and  $\lambda_{\text{geo}}$  are set to 0.02 and 0.005, respectively.

## 4 Experiments

### 4.1 Experimental Setup

**Dataset** To evaluate both 3D scene and semantic field reconstruction, we train our model on a combined dataset of ScanNet++ (Yeshwanth et al. 2023) and ScanNet (Dai et al. 2017), comprising 1565 scenes. Evaluation is conducted on 40 unseen scenes from ScanNet. Furthermore, to evaluate rendering quality, we train our model on the RealEstate10K (Zhou et al. 2018) and ACID (Liu et al. 2021) datasets. For cross-domain generalization ability, we evaluate our method on the DTU (Jensen et al. 2014) and ScanNet++ (Yeshwanth et al. 2023) benchmarks (please refer to the supplementary material).

**Implementation Details** We use DINOv2 (Oquab et al. 2024) as the image encoder, with a patch size of 16, and set the Cross-View Transformer layers as  $L = 24$ . We initialize the encoder and decoder with the weights from the pretrained VGGT (Wang et al. 2025), while the remaining intrinsic layer and Gaussian head are randomly initialized. For a fair comparison with the baseline models, we report all quantitative results under  $256 \times 256$ . Our model is implemented using PyTorch (Paszke et al. 2019) with a maximum image input length of  $N = 16$ . All experiments are conducted on  $8 \times \text{A100 GPUs}$ , taking approximately 22 hours for the training of 2 views, with a batch size of 2. Please refer to the supplementary material for further details.

### 4.2 Experiment Results

**Semantic 3D Reconstruction** As presented in Table 1 and Fig. 3, Uni3R establishes a new state-of-the-art across multiple 3D tasks, and produces remarkably coherent and precise semantic interpretations. Critically, Uni3R does not merely replicate the features of LSeg for alignment, it significantly improves upon it attributed to the robust 3D geometric priors. Furthermore, while methods like LSM necessitate ground-truth point clouds for supervision during training, Uni3R completely obviates the reliance, underscoring its enhanced practicality and scalability for real-world applications.

**Per-Scene Optimized Methods on 3D Semantic Reconstruction** To evaluate efficiency and generalization, we compare Uni3R with the per-scene optimized Feature 3DGS (Zhou et al. 2024). Such methods rely on Structure-from-Motion (Dellaert et al. 2000) to estimate camera poses, leading to high computational overhead and poor scalability. In contrast, as shown in Table 2, Uni3R demonstrates strong generalization by reconstructing consistent 3D geometry and semantics from unposed multiview inputs, while reducing reconstruction time to approximately 0.6 seconds.

**Two View Novel-View Synthesis** As shown in Table 3, Uni3R outperforms pose-dependent methods, such as PixelSplat and MVsplat, by a clear margin (1.7dB), and slightly surpasses NoPoSplat with a gain of 0.2dB on the RE10k dataset for novel view synthesis.

**Multi-View Novel-View Synthesis** Fig. 4 demonstrates Uni3R consistently produces more detailed and structurally coherent constructions. For example, in the Pool Scene, it recovers the forest area with sharper geometry, while VicaSplat shows blurring and discontinuities. These results highlight Uni3R’s ability to preserve fine details and structural consistency in pose-free multi-view 3D reconstruction. The quantitative results in Table 4 further validate the effectiveness of Uni3R in aggregating information across multiple views. Uni3R consistently outperforms all baselines under both 4-view and 8-view settings, achieving the highest PSNR. Notably, our method achieves an average improvement of 2.0 dB over VicaSplat (Li et al. 2025b), a strong sequential baseline designed for unposed video input, highlighting the superior generalization and multi-view integration capabilities of Uni3R. For NoPoSplat (Ye et al. 2025), we report the results directly from the VicaSplat paper.

**Ablation Study on Different Input View Numbers** To isolate the effect of input view quantity, we fix the view range and evaluate the reconstruction quality across varying numbers of input views. As shown in Table 5, Uni3R consistently improves in appearance, geometry, and semantic accuracy with more views. Unlike Vicasplat (Li et al. 2025b), which focuses solely on sequential rendering, and LSM (Fan et al. 2024), which reconstructs semantic and radiance fields but is restricted to two-view inputs, Uni3R is the first unified model to jointly reconstruct radiance and semantic fields from unposed multiview images. This experiment highlights Uni3R’s ability to handle long sequences and wide-baseline configurations, producing high-fidelity and semantically consistent 3D reconstructions in a single feed-forward pass.

**Ablation Study on Our Modules** We perform ablations on Uni3R, including semantic, photometric, and geometric supervision (see Table 6). Removing semantic loss leads to a collapse in mIoU, highlighting its necessity for open-vocabulary learning. Without rendering loss, the model fails to converge, confirming its central role in both synthesis and semantic guidance. Removing geometry loss degrades 3D consistency, confirming its role in depth alignment. Moreover, removing the scale-invariant constraint results in rendering quality, showing its stable optimization across scenes with varying depth scales. In general, these results highlight that Uni3R’s unified training of semantic, radiance, and geometric fields is critical to achieving high-fidelity, consistent 3D semantic reconstruction.

## 5 Conclusion

We present Uni3R, a generalizable framework for unified 3D reconstruction and semantic understanding from unposed multi-view images. It predicts a Gaussian-based scene representation that integrates appearance, geometry, and open-vocabulary semantics in a single forward pass. To address geometric inaccuracies under RGB-only supervision, we introduce a geometry-guided loss that enhances depth consistency without compromising rendering quality. Uni3R takes a significant step toward scalable, multi-view 3D scene understanding for real-world applications.

Method	Feed-Forward	8 views							16 views						
		Time↓	PSNR↑	SSIM↑	mIoU↑	Acc.↑	rel↓	$\tau$ ↑	Time↓	PSNR↑	SSIM↑	mIoU↑	Acc.↑	rel↓	$\tau$ ↑
Feature-3DGS	✗	$\approx 40min$	18.17	0.674	0.195	0.724	17.28	13.31	$\approx 60min$	17.09	0.649	0.198	0.672	23.71	10.57
<b>Ours</b>	✓	<b>0.359s</b>	<b>24.12</b>	<b>0.829</b>	<b>0.554</b>	<b>0.807</b>	<b>4.46</b>	<b>56.88</b>	<b>0.636s</b>	<b>23.07</b>	<b>0.806</b>	<b>0.522</b>	<b>0.795</b>	<b>5.88</b>	<b>42.88</b>

Table 2: Comparison with Per-Scene Optimized Methods. Time corresponds to the average reconstruction time per scene.

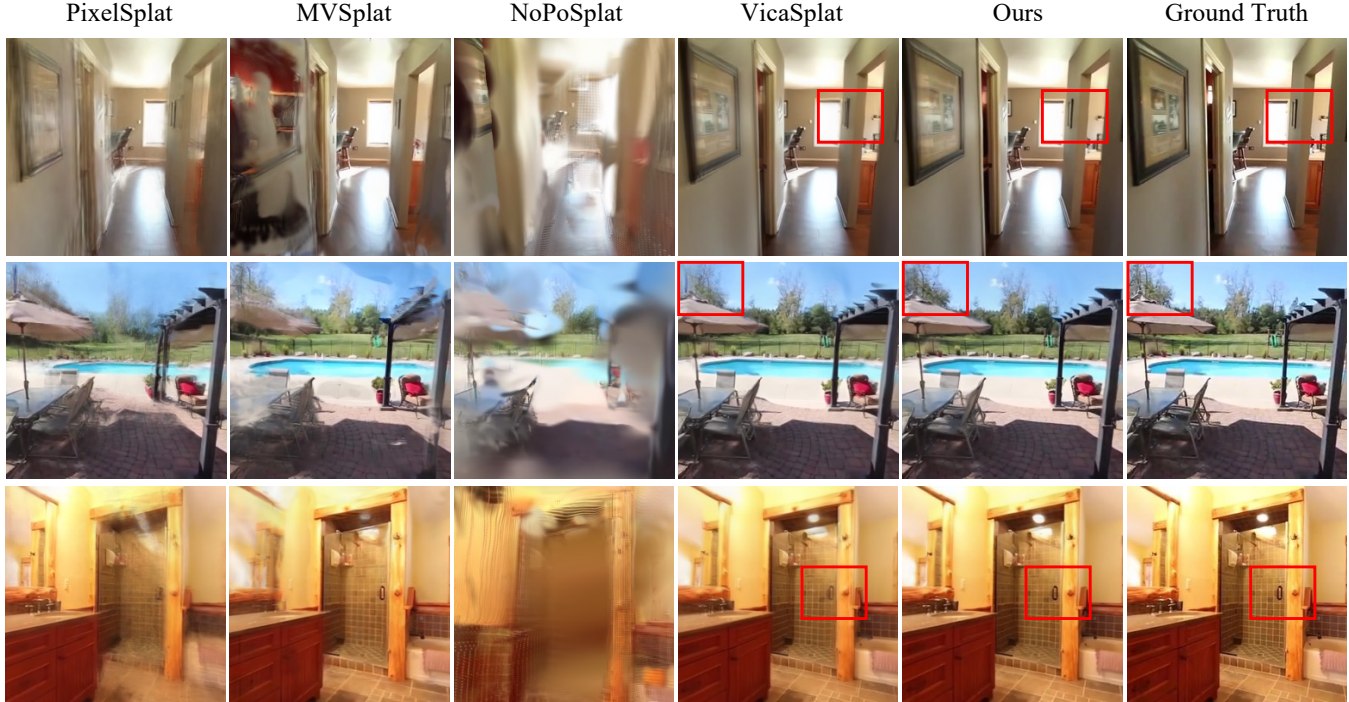


Figure 4: Qualitative comparison of novel view synthesis on RealEstate10k test set with 8 input images.

Method	RE10k			ACID		
	PSNR↑	SSIM↑	LPIPS↓	PSNR↑	SSIM↑	LPIPS↓
<i>Pose-Required</i>						
PixelSplat	23.361	0.803	0.186	25.684	0.778	0.194
MV3Splat	23.430	0.805	0.179	25.335	0.772	0.195
<i>Pose-Free</i>						
NoPoSplat	25.036	<b>0.838</b>	0.162	<b>25.961</b>	<b>0.781</b>	<b>0.189</b>
CoPoNeRF	18.938	0.619	0.388	20.950	0.606	0.406
VicaSplat	25.038	0.834	0.161	25.439	0.757	0.201
<b>Ours</b>	<b>25.074</b>	<b>0.837</b>	<b>0.158</b>	<b>25.766</b>	<b>0.778</b>	<b>0.192</b>

Table 3: Quantitative comparisons of novel view synthesis on the RE10k and ACID dataset under 2-views setup.

## References

Bleyer, M.; Rhemann, C.; and Rother, C. 2011. PatchMatch Stereo - Stereo Matching with Slanted Support Windows. In *British Machine Vision Conference, BMVC 2011, Dundee, UK, August 29 - September 2, 2011. Proceedings*, 1–11.

Charatan, D.; Li, S. L.; Tagliasacchi, A.; and Sitzmann, V. 2024. PixelSplat: 3D Gaussian Splats from Image Pairs for Scalable Generalizable 3D Reconstruction. In *IEEE/CVF Conference on Computer Vision and Pattern Recognition*,

*CVPR 2024, Seattle, WA, USA, June 16-22, 2024*, 19457–19467.

Chen, A.; Xu, Z.; Zhao, F.; Zhang, X.; Xiang, F.; Yu, J.; and Su, H. 2021. MVSNeRF: Fast Generalizable Radiance Field Reconstruction from Multi-View Stereo. In *2021 IEEE/CVF International Conference on Computer Vision, ICCV 2021, Montreal, QC, Canada, October 10-17, 2021*, 14104–14113.

Chen, Y.; Xu, H.; Zheng, C.; Zhuang, B.; Pollefeys, M.; Geiger, A.; Cham, T.; and Cai, J. 2024. MV3Splat: Efficient 3D Gaussian Splatting from Sparse Multi-view Images. In *Computer Vision - ECCV 2024 - 18th European Conference, Milan, Italy, September 29-October 4, 2024, Proceedings, Part XXI*, 370–386.

Dai, A.; Chang, A. X.; Savva, M.; Halber, M.; Funkhouser, T. A.; and Nießner, M. 2017. ScanNet: Richly-Annotated 3D Reconstructions of Indoor Scenes. In *2017 IEEE Conference on Computer Vision and Pattern Recognition, CVPR 2017, Honolulu, HI, USA, July 21-26, 2017*, 2432–2443.

Dellaert, F.; Seitz, S. M.; Thorpe, C. E.; and Thrun, S. 2000. Structure from Motion without Correspondence. In *2000 Conference on Computer Vision and Pattern Recognition*

		4 views (RE10k)			8 views (RE10k)			4 views (ScanNet)			8 views (ScanNet)		
Method		PSNR $\uparrow$	SSIM $\uparrow$	LPIPS $\downarrow$	PSNR $\uparrow$	SSIM $\uparrow$	LPIPS $\downarrow$	PSNR $\uparrow$	SSIM $\uparrow$	LPIPS $\downarrow$	PSNR $\uparrow$	SSIM $\uparrow$	LPIPS $\downarrow$
<i>Pose-Required</i>	PixelSplat	20.459	0.729	0.267	19.734	0.694	0.290	21.185	0.712	0.351	18.582	0.637	0.440
	MVSplat	20.882	0.761	0.233	19.726	0.743	0.262	14.946	0.472	0.544	13.061	0.407	0.608
<i>Pose-Free</i>	NoPoSplat	16.299	0.552	0.397	14.372	0.469	0.520	16.940	0.560	0.425	12.939	0.397	0.588
	CoPoNeRF	18.299	0.655	0.559	18.984	0.692	0.553	20.247	0.775	0.535	19.821	0.772	0.542
	Vicasplat	24.537	0.814	0.162	24.502	0.806	0.164	26.673	0.856	0.188	23.656	0.777	0.262
	<b>Ours</b>	<b>26.360</b>	<b>0.866</b>	<b>0.129</b>	<b>26.629</b>	<b>0.874</b>	<b>0.118</b>	<b>28.324</b>	<b>0.891</b>	<b>0.161</b>	<b>26.019</b>	<b>0.858</b>	<b>0.193</b>

Table 4: Comparison with 4 and 8-view settings on the RE10k (Zhou et al. 2018) and ScanNet (Dai et al. 2017) datasets.

View Num	mIoU $\uparrow$	Acc. $\uparrow$	rel $\downarrow$	$\tau$ $\uparrow$	PSNR $\uparrow$	SSIM $\uparrow$	LPIPS $\downarrow$
4 views	0.523	0.749	9.9	31.4	16.43	0.675	0.418
8 views	0.593	0.821	5.6	48.4	21.15	0.767	0.336
16 views	0.629	0.834	4.7	51.4	23.36	0.808	0.294

Table 5: Ablation Study on Input View numbers. We fix the view range and evaluate the reconstruction quality under varying numbers of input views.

Method	mIoU $\uparrow$	rel $\downarrow$	$\tau$ $\uparrow$	PSNR $\uparrow$	SSIM $\uparrow$
frozen all transformer layers	0.0634	51.1	7.6	5.49	0.052
w/o semantic loss	0.0183	5.8	47.4	25.38	0.869
w/o rendering loss	0.2653	N/A	N/A	N/A	N/A
w/o scale invariant	0.5382	5.8	47.9	24.95	0.861
w/o intrinsic embedding	0.5471	6.5	42.5	25.35	0.871
w/o geo. loss	<b>0.5541</b>	5.6	48.2	<b>25.53</b>	0.872
<b>Ours</b>	0.5484	<b>3.9</b>	<b>61.2</b>	<b>25.53</b>	<b>0.873</b>

Table 6: Ablation Study on different modules. We evaluate the ablated variants of Uni3R, by recording their rendering quality, segmentation performance and geometric accuracy.

(CVPR 2000), 13-15 June 2000, Hilton Head, SC, USA, 2557–2564.

Fan, Z.; Zhang, J.; Cong, W.; Wang, P.; Li, R.; Wen, K.; Zhou, S.; Kadambi, A.; Wang, Z.; Xu, D.; Ivanovic, B.; and Pavone, M. 2024. Large Spatial Model: End-to-end Unposed Images to Semantic 3D. In *Advances in Neural Information Processing Systems 38: Annual Conference on Neural Information Processing Systems 2024, NeurIPS 2024, Vancouver, BC, Canada, December 10 - 15, 2024*.

Jensen, R. R.; Dahl, A. L.; Vogiatzis, G.; Tola, E.; and Aanaes, H. 2014. Large Scale Multi-view Stereopsis Evaluation. In *2014 IEEE Conference on Computer Vision and Pattern Recognition, CVPR 2014, Columbus, OH, USA, June 23-28, 2014*, 406–413. IEEE Computer Society.

Jiang, H.; Liu, L.; Cheng, T.; Wang, X.; Lin, T.; Su, Z.; Liu, W.; and Wang, X. 2025. GaussTR: Foundation Model-Aligned Gaussian Transformer for Self-Supervised 3D Spatial Understanding. In *IEEE/CVF Conference on Computer Vision and Pattern Recognition, CVPR 2025, Nashville, TN, USA, June 11-15, 2025*, 11960–11970.

Kang, G.; Nam, S.; Sun, X.; Khamis, S.; Mohamed, A.; and

Park, E. 2025. iLRM: An Iterative Large 3D Reconstruction Model. arXiv:2507.23277.

Kerbl, B.; Kopanas, G.; Leimkühler, T.; and Drettakis, G. 2023. 3D Gaussian Splatting for Real-Time Radiance Field Rendering. *ACM Trans. Graph.*, 42(4): 139:1–139:14.

Kerr, J.; Kim, C. M.; Goldberg, K.; Kanazawa, A.; and Tancik, M. 2023. LERF: Language Embedded Radiance Fields. In *IEEE/CVF International Conference on Computer Vision, ICCV 2023, Paris, France, October 1-6, 2023*, 19672–19682.

Leroy, V.; Cabon, Y.; and Revaud, J. 2024. Grounding Image Matching in 3D with MAST3R. In *Computer Vision - ECCV 2024 - 18th European Conference, Milan, Italy, September 29-October 4, 2024, Proceedings, Part LXXII*, volume 15130, 71–91.

Li, B.; Weinberger, K. Q.; Belongie, S. J.; Koltun, V.; and Ranftl, R. 2022. Language-driven Semantic Segmentation. In *The Tenth International Conference on Learning Representations, ICLR 2022, Virtual Event, April 25-29, 2022*.

Li, Y.; Cheng, T.; Feng, B.; Liu, W.; and Wang, X. 2025a. Mask-Adapter: The Devil is in the Masks for Open-Vocabulary Segmentation. In *IEEE/CVF Conference on Computer Vision and Pattern Recognition, CVPR 2025, Nashville, TN, USA, June 11-15, 2025*, 14998–15008. Computer Vision Foundation / IEEE.

Li, Z.; Dong, C.; Chen, Y.; Huang, Z.; and Liu, P. 2025b. VicaSplat: A Single Run is All You Need for 3D Gaussian Splatting and Camera Estimation from Unposed Video Frames. *CoRR*, abs/2503.10286.

Liang, S.; Wang, S.; Li, K.; Niemeyer, M.; Gasperini, S.; Navab, N.; and Tombari, F. 2024. Supergseg: Open-vocabulary 3d segmentation with structured super-gaussians. *arXiv preprint arXiv:2412.10231*.

Liu, A.; Makadia, A.; Tucker, R.; Snavely, N.; Jampani, V.; and Kanazawa, A. 2021. Infinite Nature: Perpetual View Generation of Natural Scenes from a Single Image. In *2021 IEEE/CVF International Conference on Computer Vision, ICCV 2021, Montreal, QC, Canada, October 10-17, 2021*, 14438–14447. IEEE.

Liu, T.; Wang, G.; Hu, S.; Shen, L.; Ye, X.; Zang, Y.; Cao, Z.; Li, W.; and Liu, Z. 2024. Mvsgaussian: Fast generalizable gaussian splatting reconstruction from multi-view stereo. In *European Conference on Computer Vision*, 37–53. Springer.

- Mildenhall, B.; Srinivasan, P. P.; Tancik, M.; Barron, J. T.; Ramamoorthi, R.; and Ng, R. 2020. NeRF: Representing Scenes as Neural Radiance Fields for View Synthesis. In *Computer Vision - ECCV 2020 - 16th European Conference, Glasgow, UK, August 23-28, 2020, Proceedings, Part I*, 405–421.
- Nam, S.; Sun, X.; Kang, G.; Lee, Y.; Oh, S.; and Park, E. 2025. Generative Densification: Learning to Densify Gaussians for High-Fidelity Generalizable 3D Reconstruction. In *IEEE/CVF Conference on Computer Vision and Pattern Recognition, CVPR 2025, Nashville, TN, USA, June 11-15, 2025*, 26683–26693. Computer Vision Foundation / IEEE.
- Oquab, M.; Darcet, T.; Moutakanni, T.; Vo, H. V.; Szafraniec, M.; Khalidov, V.; Fernandez, P.; Haziza, D.; Massa, F.; El-Nouby, A.; Assran, M.; Ballas, N.; Galuba, W.; Howes, R.; Huang, P.; Li, S.; Misra, I.; Rabbat, M.; Sharma, V.; Synnaeve, G.; Xu, H.; Jégou, H.; Mairal, J.; Labatut, P.; Joulin, A.; and Bojanowski, P. 2024. DINOv2: Learning Robust Visual Features without Supervision. *Trans. Mach. Learn. Res.*
- Paszke, A.; Gross, S.; Massa, F.; Lerer, A.; Bradbury, J.; Chanan, G.; Killeen, T.; Lin, Z.; Gimelshein, N.; Antiga, L.; Desmaison, A.; Köpf, A.; Yang, E. Z.; DeVito, Z.; Raison, M.; Tejani, A.; Chilamkurthy, S.; Steiner, B.; Fang, L.; Bai, J.; and Chintala, S. 2019. PyTorch: An Imperative Style, High-Performance Deep Learning Library. In *Advances in Neural Information Processing Systems 32: Annual Conference on Neural Information Processing Systems 2019, NeurIPS 2019, December 8-14, 2019, Vancouver, BC, Canada*, 8024–8035.
- Qin, M.; Li, W.; Zhou, J.; Wang, H.; and Pfister, H. 2024. LangSplat: 3D Language Gaussian Splatting. In *IEEE/CVF Conference on Computer Vision and Pattern Recognition, CVPR 2024, Seattle, WA, USA, June 16-22, 2024*, 20051–20060.
- Radford, A.; Kim, J. W.; Hallacy, C.; Ramesh, A.; Goh, G.; Agarwal, S.; Sastry, G.; Askell, A.; Mishkin, P.; Clark, J.; Krueger, G.; and Sutskever, I. 2021. Learning Transferable Visual Models From Natural Language Supervision. In *Proceedings of the 38th International Conference on Machine Learning, ICML 2021, 18-24 July 2021, Virtual Event*, 8748–8763.
- Ranftl, R.; Bochkovskiy, A.; and Koltun, V. 2021. Vision Transformers for Dense Prediction. In *2021 IEEE/CVF International Conference on Computer Vision, ICCV 2021, Montreal, QC, Canada, October 10-17, 2021*, 12159–12168.
- Shi, D.; Wang, W.; Chen, D. Y.; Zhang, Z.; Bian, J.; Zhuang, B.; and Shen, C. 2025. Revisiting Depth Representations for Feed-Forward 3D Gaussian Splatting. *CoRR*, abs/2506.05327.
- Smart, B.; Zheng, C.; Laina, I.; and Prisacariu, V. A. 2024. Splat3R: Zero-shot Gaussian Splatting from Uncalibrated Image Pairs. *CoRR*, abs/2408.13912.
- Tian, Q.; Tan, X.; Gong, J.; Xie, Y.; and Ma, L. 2025. UniForward: Unified 3D Scene and Semantic Field Reconstruction via Feed-Forward Gaussian Splatting from Only Sparse-View Images. *CoRR*, abs/2506.09378.
- Umeyama, S. 1991. Least-Squares Estimation of Transformation Parameters Between Two Point Patterns. *IEEE Trans. Pattern Anal. Mach. Intell.*, 13(4): 376–380.
- Wang, J.; Chen, M.; Karaev, N.; Vedaldi, A.; Rupprecht, C.; and Novotný, D. 2025. VGGT: Visual Geometry Grounded Transformer. In *IEEE/CVF Conference on Computer Vision and Pattern Recognition, CVPR 2025, Nashville, TN, USA, June 11-15, 2025*, 5294–5306.
- Wang, S.; Leroy, V.; Cabon, Y.; Chidlovskii, B.; and Revaud, J. 2024a. DUST3R: Geometric 3D Vision Made Easy. In *IEEE/CVF Conference on Computer Vision and Pattern Recognition, CVPR 2024, Seattle, WA, USA, June 16-22, 2024*, 20697–20709.
- Wang, X.; Lan, C.; Zhu, H.; Chen, Z.; and Lu, Y. 2024b. GSemSplat: Generalizable Semantic 3D Gaussian Splatting from Uncalibrated Image Pairs. *arXiv preprint arXiv:2412.16932*.
- Xu, H.; Peng, S.; Wang, F.; Blum, H.; Barath, D.; Geiger, A.; and Pollefeys, M. 2025. DepthSplat: Connecting Gaussian Splatting and Depth. In *IEEE/CVF Conference on Computer Vision and Pattern Recognition, CVPR 2025, Nashville, TN, USA, June 11-15, 2025*, 16453–16463. Computer Vision Foundation / IEEE.
- Ye, B.; Liu, S.; Xu, H.; Li, X.; Pollefeys, M.; Yang, M.; and Peng, S. 2025. No Pose, No Problem: Surprisingly Simple 3D Gaussian Splats from Sparse Unposed Images. In *The Thirteenth International Conference on Learning Representations, ICLR 2025, Singapore, April 24-28, 2025*.
- Yeshwanth, C.; Liu, Y.; Nießner, M.; and Dai, A. 2023. ScanNet++: A High-Fidelity Dataset of 3D Indoor Scenes. In *IEEE/CVF International Conference on Computer Vision, ICCV 2023, Paris, France, October 1-6, 2023*, 12–22. IEEE.
- Yu, A.; Ye, V.; Tancik, M.; and Kanazawa, A. 2021. pixel-NeRF: Neural Radiance Fields From One or Few Images. In *IEEE Conference on Computer Vision and Pattern Recognition, CVPR 2021, virtual, June 19-25, 2021*, 4578–4587.
- Zhai, H.; Li, H.; Li, Z.; Pan, X.; He, Y.; and Zhang, G. 2025. Panogs: Gaussian-based panoptic segmentation for 3d open vocabulary scene understanding. In *Proceedings of the Computer Vision and Pattern Recognition Conference*, 14114–14124.
- Zhang, R.; Isola, P.; Efros, A. A.; Shechtman, E.; and Wang, O. 2018. The Unreasonable Effectiveness of Deep Features as a Perceptual Metric. In *2018 IEEE Conference on Computer Vision and Pattern Recognition, CVPR 2018, Salt Lake City, UT, USA, June 18-22, 2018*, 586–595. Computer Vision Foundation / IEEE Computer Society.
- Zhou, S.; Chang, H.; Jiang, S.; Fan, Z.; Zhu, Z.; Xu, D.; Chari, P.; You, S.; Wang, Z.; and Kadambi, A. 2024. Feature 3DGS: Supercharging 3D Gaussian Splatting to Enable Distilled Feature Fields. In *IEEE/CVF Conference on Computer Vision and Pattern Recognition, CVPR 2024, Seattle, WA, USA, June 16-22, 2024*, 21676–21685.

Zhou, T.; Tucker, R.; Flynn, J.; Fyffe, G.; and Snavely, N. 2018. Stereo magnification: Learning view synthesis using multiplane images. *arXiv preprint arXiv:1805.09817*.